Short-range order in Cu-Pd alloys

1992 J. Phys.: Condens. Matter 4 10093

(http://iopscience.iop.org/0953-8984/4/49/037)

J. Phys.: Condens. Matter 4 (1992) 10093–10102. Printed in the UK

Short-range order in Cu–Pd alloys

Dilip Kumar Saha, Kenji Koga and Ken-ichi Ohshima
Institute of Applied Physics, University of Tsukuba, Tsukuba 305, Japan

Received 16 March 1992, in final form 15 June 1992

Abstract. The x-ray diffuse scattering intensity was measured at room temperature from disordered Cu–Pd alloys containing 8.0, 9.5, 13.0, 21.8, 28.5 and 42.0 at.% Pd. Twofold and fourfold splittings of diffuse scattering due to short-range order (SRO) were observed at 100, 110 and their equivalent positions respectively from alloys with more than 13.0 at.% Pd, where the separation of the split diffuse maxima increases monotonically with increasing Pd content. No splitting of diffuse scattering was observed for alloys containing 13.0 at.% Pd or less. The diffuse intensities measured in Laue units increase with increasing Pd content except for 42.0 at.% Pd alloy, which shows a much lower intensity compared with that for 28.5 at.% Pd alloy. The SRO parameters were determined from all the six alloys. One representative set of the local atomic arrangements of Pd atoms in the FCC lattice which has been derived from computer simulation of the observed SRO parameters is shown. We have calculated the Pd–Pd atom pairs of the first- and second-nearest neighbours for all the six alloys, in both the random and the SRO case. Although the ordered structure for Cu–42.0 at.% Pd alloy is of the CsCl type, no different feature in the SRO structure was observed for this alloy in comparison with the other alloys.

1. Introduction

It is important to measure the short-range order (SRO) diffuse scattering intensity from materials to understand inherent structural fluctuations. In the Cu–Pd alloy system, the SRO diffuse scattering from the disordered state has been studied qualitatively by electron diffraction in the Pd concentration range from about 13.0 to 60.0 at.%, where the characteristic twofold and fourfold splitting diffuse maxima were observed at around 100, 110 and their equivalent positions in reciprocal space (Ohshima and Watanabe 1973). The result was interpreted in terms of the Fermi surface imaging theory proposed by Krivoglaz (1969) and it was concluded that the pair interaction potential in this alloy system mainly originates from conduction electrons, and diffuse scattering reflects the flat section of the Fermi surface. X-ray studies have been performed quantitatively for only one alloy of this system, namely Cu–29.8 at.% Pd (Ohshima *et al* 1976).

Gyorffy and Stocks (1983) calculated the Fermi surfaces for the disordered Cu–Pd alloys on the basis of self-consistent-field KKR CPA calculation. They argued that the observed composition-dependent peaks in the electron and x-ray diffuse scattering intensities are due to parallel sheets of flat Fermi surface and the positions of the peak are directly related to the Fermi vector. Rao *et al* (1984) also calculated the electronic structure of copper-rich Cu–Pd alloys with a KKR CPA computation. Takano *et al* (1991) have discussed the effect of SRO on the electronic structure of disordered

0953-8984/92/4910093+10$07.50

Cu–50 at.% Pd alloy. They pointed out that the SRO should be considered when the band-structure energy is calculated in the disordered state.

It is well known that the Cu–Pd alloy system forms a continuous series of solid solutions with FCC structure at elevated temperatures (Massalski *et al* 1990). Below the composition-dependent critical temperature T_c, various types of superlattice structure are formed. The alloys with Pd concentrations from 18 to 28 at.% (α''-phase alloys) have periodic one-dimensional ($L1_{2-S}$ type) or two-dimensional ($L1_{2-S1,S2}$ type) anti-phase domain structures in the ordered state, depending on the composition and temperature, the fundamental cell of which consists of a face-centred tetragonal atomic arrangement of the ordered Cu_3Au type. The alloys with a Pd content less than 18 at.% (α'-phase alloys) have the ordered Cu_3Au-type structure with cubic symmetry. The β-phase, having the CsCl-type structure, was found for alloys with between 36 and 46 at.% Pd.

It is, therefore, of great interest to obtain a series of composition-dependent SRO diffuse intensities and SRO parameters using x-ray diffuse scattering techniques for the disordered Cu–Pd alloys to understand local atomic arrangements. In particular, there are no reports on the nature of diffuse scattering from alloys with around 40 at.% Pd and on the shape of diffuse scattering from alloys with less than 13 at.% Pd. In the present paper, we have measured the x-ray diffuse intensities from six disordered Cu–Pd alloys. The SRO parameters were determined after analysing the composition-dependent diffuse intensities. Local atomic arrangements of Pd atoms were constructed and the numbers of Pd–Pd atom pairs of first- and second-nearest neighbours have been tabulated.

2. Experimental details

Alloys with different compositions were prepared by melting 99.99% pure Cu and Pd in evacuated silica tubes and remelting several times to homogenize them. Single crystals were grown by the Bridgman technique. Sample slices of different dimensions from 10 mm × 8 mm × 3 mm to 12 mm × 10 mm × 3 mm were cut parallel to a (210) plane from their original ingots. The slices were polished mechanically and etched chemically and electrically to remove the distorted surface layer. For Cu–21.8 at.% Pd, Cu–28.5 at.% Pd and Cu–42.0 at.% Pd alloys, electrical etching was performed using a solution consisting of 90% C_2H_5OH and 10% HCl with a graphite cathode. Chemical etching was performed for Cu–13.0 at.% Pd using a solution consisting of 30% HNO_3, 10% HCl, 10% H_3PO_4 and 50% CH_3COOH, and for Cu–8.0 at.% Pd and Cu–9.5 at.% Pd alloys using a solution consisting of 90% HNO_3 and 10% H_2O. All the specimens were annealed separately in evacuated silica tubes at 900 °C for 4 d, 800 °C for 1 d and 750 °C for 10 d successively to homogenize the specimens and finally quenched by dropping them into ice–water. The alloy with 42.0 at.% Pd could not be annealed because it has a CsCl-type structure at low temperatures. The surface of the specimens was etched again to remove the oxide layer.

The lattice parameters of the specimens, which were prepared separately, were measured with an x-ray Debye–Scherrer camera using Cu Kα radiation. The specimen compositions were determined with an accuracy of ±0.3 at.% by comparison with the lattice parameter versus composition relation (Pearson 1958). The six compositions were determined as Cu–8.0 at.% Pd, Cu–9.5 at.% Pd, Cu–13.0 at.% Pd, Cu–21.8 at.% Pd, Cu–28.5 at.% Pd and Cu–42.0 at.% Pd.

The x-ray intensity measurements were performed at room temperature using a four-circle goniometer attached to a rota-unit of an x-ray generator (Rigaku RU-300). The incident-beam Cu Kα radiation from a Cu target was monochromated by a singly bent HOPG crystal. In order to eliminate the $\lambda/2$ harmonics, a Ross balanced-filter technique was used. The diffuse intensities were measured by scanning a volume of reciprocal space at intervals of $\Delta h_i = \frac{1}{40}$ in terms of the distance between the 000 and 200 fundamental spots. Both background and air scattering were estimated by irradiating an Si single crystal and were subtracted from the measured intensity. The procedure for the x-ray diffuse intensity analysis was the same as that used in the study of Au–Cr alloys (Koga and Ohshima 1990).

3. Results and discussion

The SRO diffuse intensity distributions in Laue units for all the six alloys are shown on the $(hk0)$ reciprocal lattice plane in figure 1. As seen in figures 1(*d*)–(*f*), twofold splitting at the 100 position and fourfold splitting at the 110 position appeared. The separation between the split diffuse maxima at the 110 position relative to the distance between the two fundamental spots 000 and 200, which was denoted by m and defined in figure 1(*f*), was measured for the samples and is shown in table 1. The distance m shows a monotonic increase with increasing Pd content. The separation m was estimated from the energy band-structure calculation by Gyorffy and Stocks (1983) and these values are also given in table 1. The agreement between the two is fairly good. On the other hand, no splittings were found in figures 1(*a*)–(*c*). The separation m for the 8.0 and 9.5 at.% Pd alloys should be very small on the basis of the simple model used by Ohshima and Watanabe (1973). Because of the weak SRO diffuse intensities for the two alloys, it was difficult to obtain the value of the split diffuse maxima. To compare the intensity maxima and to see their splittings clearly, bird's-eye views of figure 1 are shown in figure 2. In particular, the small value of m is visible in figure 2(*d*), but it is not obvious in figure 1(*d*). As seen in figure 2, the SRO diffuse intensity increases with increasing Pd content except for the Cu–42.0 at.% Pd alloy, which has a much lower intensity. We could not observe any extra diffuse scattering in addition to split diffuse scattering for the Cu–42.0 at.% Pd alloy.

Table 1. Values of the separation m measured in terms of the distance between the 000 and 200 spots and those estimated from the band calculation.

Pd content (at.%)	m measured in quenched state	m estimated from the band calculation by Gyorffy and Stocks (1983)
8.0	0	—
9.5	0	—
13.0	0	0.010
21.8	0.042±0.005	0.060±0.01
28.5	0.107±0.005	0.120±0.01
42.0	0.201±0.005	0.225±0.01

By Fourier inversion of the SRO diffuse scattering intensities shown in figure 1, the Warren–Cowley SRO parameters α_{lmn} were determined up to the fiftieth shell

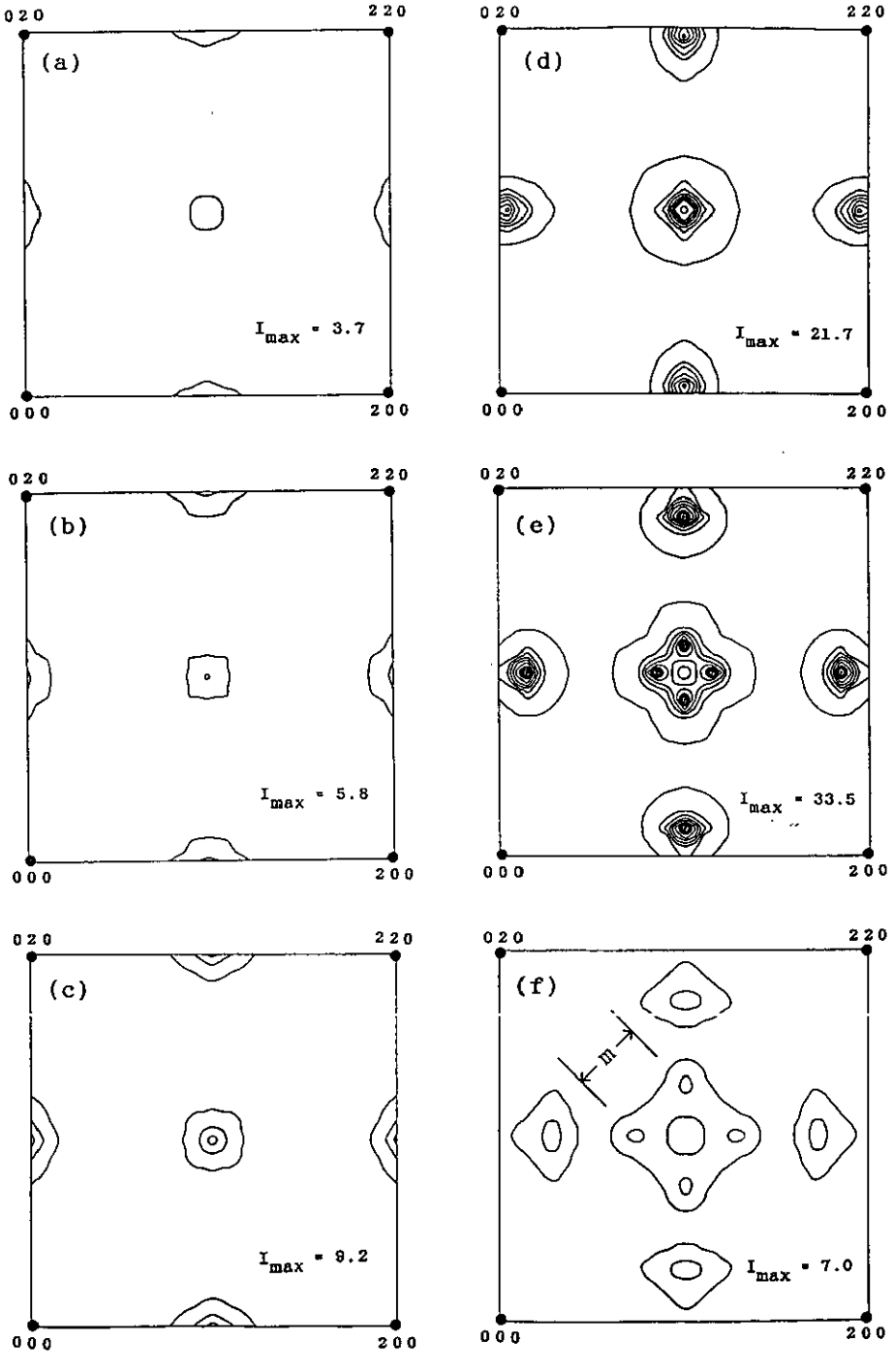

Figure 1. The SRO diffuse scattering intensity distributions on the $(h\,k0)$ reciprocal lattice plane in Laue units for (*a*) Cu–8.0 at.% Pd, (*b*) Cu–9.5 at.% Pd, (*c*) Cu–13.0 at.% Pd, (*d*) Cu–21.8 at.% Pd, (*e*) Cu–28.5 at.% Pd and (*f*) Cu–42.0 at.% Pd alloys ($I_{min} = 2.0$ and $\Delta I = 3.0$ Laue units).

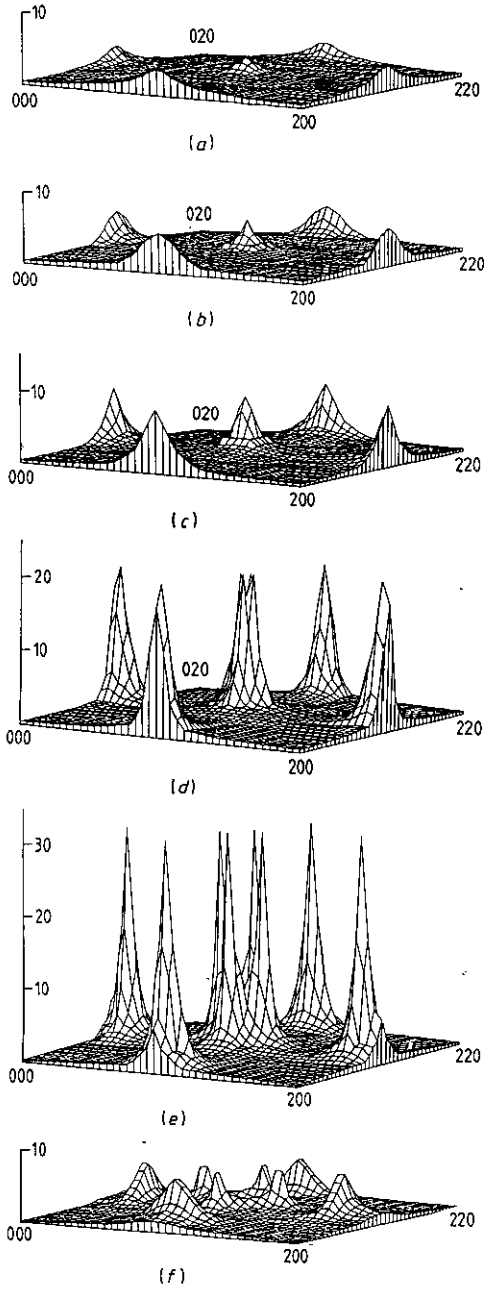

Figure 2. Bird's-eye views of figure 1.

for all the six disordered Cu–Pd alloys, with an error estimated to be less than $\pm 10\%$. These values are listed in table 2, where l, m and n are integers. The values of α_{000} are very close to unity for all the data. The absolute values of α_{lmn} become smaller with decreasing Pd content from the 28.5 at.% Pd alloy. It is thought that the SRO state has a tendency to become more random with decreasing Pd content. However,

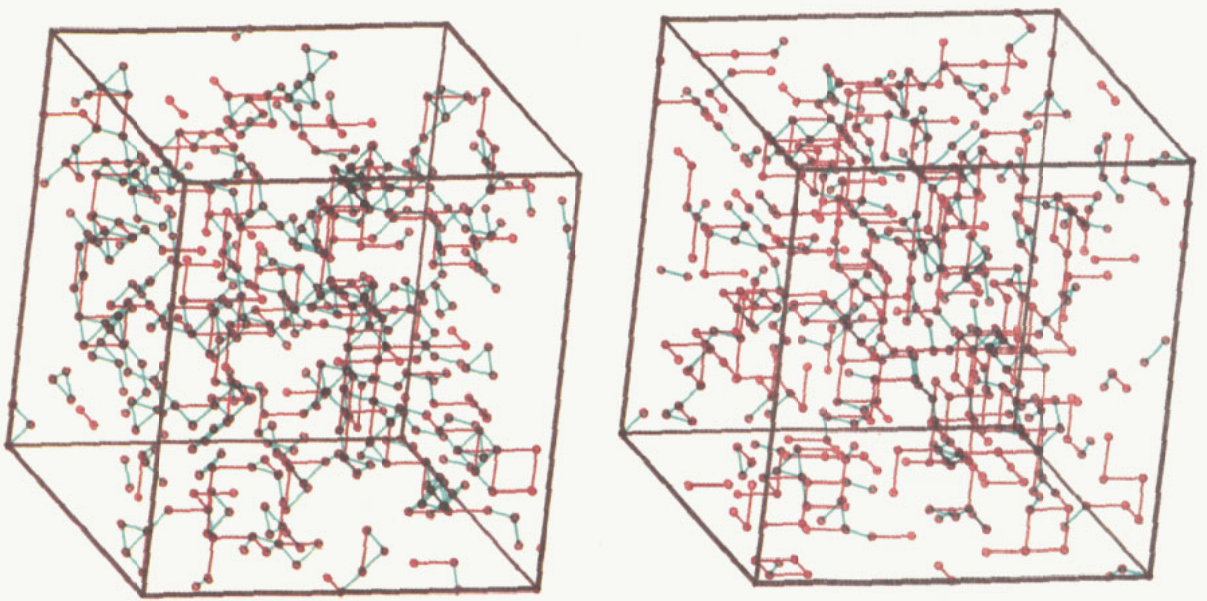

(a) (b)

Figure 3.Three-dimensional distributions of Pd atoms simulated on 10 × 10 × 10 FCC unit cells for Cu–13.0 at.% Pd alloy: (*a*) for an ideally random state; (*b*) for the observed SRO structure. Pd atoms are represented by circles and these are linked together by red and green solid lines to their first- and second-nearest neighbours, respectively.

Table 2. SRO parameters α_{lmn} determined from the Fourier transform of the SRO diffuse scattering intensities and one set of these parameters for Cu–13.0 at.% Pd alloy calculated from the model by computer simulation where N is the shell number.

		SRO parameter α_{lmn}						
				13.0 at.% Pd				
N	lmn	8.0 at.% Pd	9.5 at.% Pd	Experiment	Simulation	21.8 at.% Pd	28.5 at.% Pd	42.0 at.% Pd
	000	1.023	1.010	1.009	1.000	1.018	1.014	1.017
1	110	−0.003	−0.021	−0.073	−0.072	−0.088	−0.157	−0.144
2	200	0.046	0.055	0.091	0.090	0.152	0.171	0.125
3	211	−0.043	−0.029	−0.024	−0.024	−0.027	−0.011	−0.005
4	220	−0.020	−0.008	−0.010	−0.010	0.044	0.066	0.035
5	310	−0.016	−0.013	−0.016	−0.016	−0.026	−0.024	−0.009
6	222	0.017	0.018	0.025	0.025	0.047	0.046	0.017
7	321	0.007	0.003	0.014	0.014	−0.004	−0.008	0.007
8	400	0.017	0.008	0.007	0.006	0.045	0.033	0.002
9	330	−0.017	−0.015	−0.025	−0.025	−0.028	−0.035	−0.026
	411	0.010	0.010	0.006	0.006	−0.013	−0.013	0.001
10	420	0.013	0.008	0.018	0.017	0.028	0.044	0.016
11	332	0.005	0.002	−0.006	−0.006	−0.012	−0.013	−0.013
12	422	0.009	0.003	0.007	0.007	0.027	0.024	−0.004
13	431	−0.003	−0.004	−0.007	−0.007	−0.008	−0.007	0.005
	510	0.019	0.013	0.005	0.004	0.009	−0.005	−0.007
14	521	0.003	0.001	−0.011	−0.011	−0.011	−0.014	−0.005
15	440	−0.005	−0.003	0.005	0.005	0.017	0.009	−0.019
16	433	−0.002	0.000	−0.003	−0.003	−0.006	−0.002	0.010
	530	0.015	0.014	0.023	0.023	0.009	−0.003	0.001
17	442	−0.003	−0.002	−0.003	−0.003	0.015	0.011	−0.004
	600	−0.016	−0.014	−0.021	−0.021	−0.005	0.025	0.012
18	532	−0.002	0.003	0.005	0.005	0.000	−0.004	−0.001
	611	0.002	−0.001	0.009	0.009	−0.009	−0.015	−0.003
19	620	0.011	0.009	0.019	0.018	0.017	0.014	−0.004
20	541	−0.006	−0.005	−0.005	−0.005	−0.006	0.005	0.013
21	622	−0.005	−0.003	−0.003	−0.003	0.013	0.016	−0.001
22	631	−0.004	−0.005	−0.012	−0.013	−0.013	0.001	0.008
23	444	0.002	0.001	0.001	0.001	0.010	0.004	−0.004
24	543	−0.001	−0.001	0.002	0.002	−0.003	−0.003	−0.001
	550	−0.008	−0.006	−0.016	−0.016	−0.008	−0.013	−0.014
	710	−0.012	−0.009	−0.008	−0.008	−0.001	−0.004	−0.004
25	640	0.001	0.003	0.009	0.009	0.012	0.008	−0.008
26	552	0.001	0.002	0.001	0.001	−0.003	−0.010	−0.007
	633	0.000	0.000	−0.002	−0.002	−0.006	−0.001	0.000
	721	−0.004	−0.004	−0.003	−0.003	−0.005	0.001	0.008
27	642	0.002	0.002	0.003	0.003	0.009	0.005	−0.007
28	730	0.004	0.003	0.007	0.007	0.002	−0.008	−0.012
29	651	0.000	0.001	−0.002	−0.002	0.000	0.003	0.006
	732	0.000	0.000	−0.001	−0.001	0.000	−0.006	−0.004
30	800	−0.011	−0.005	−0.011	−0.011	0.004	0.013	0.013
31	554	0.001	−0.002	0.000	0.000	−0.004	−0.001	0.002
	741	0.003	0.000	0.003	0.003	−0.002	−0.002	0.005
	811	−0.009	−0.006	−0.002	−0.002	−0.011	−0.011	−0.006
32	644	0.002	0.001	0.002	0.002	0.008	0.004	−0.002
	820	−0.005	−0.001	0.005	0.005	0.008	0.010	0.000
33	653	0.000	−0.002	−0.003	−0.003	−0.003	0.002	0.004

Table 2. (continued)

		SRO parameter α_{lmn}						
				13.0 at.% Pd				
N	lmn	8.0 at.% Pd	9.5 at.% Pd	Experiment	Simulation	21.8 at.% Pd	28.5 at.% Pd	42.0 at.% Pd
34	660	−0.006	−0.003	−0.003	−0.003	0.003	−0.001	−0.003
	822	0.001	0.000	0.006	0.006	0.009	0.009	0.002
35	743	0.001	0.002	0.002	0.002	0.000	0.003	0.004
	750	0.002	0.001	0.001	0.001	−0.002	−0.002	0.004
	831	0.000	−0.002	−0.004	−0.004	−0.008	−0.006	0.000
36	662	0.001	0.001	0.002	0.002	0.003	−0.001	−0.001
37	752	0.003	0.003	0.003	0.003	0.000	−0.006	−0.002
38	840	0.002	0.001	0.000	0.000	0.006	0.005	−0.006
39	833	0.001	0.001	−0.004	−0.004	−0.004	−0.005	0.000
	910	0.007	0.003	−0.002	−0.002	0.001	0.000	0.001
40	842	0.000	0.001	0.001	0.001	0.006	0.001	−0.004
41	655	−0.001	−0.002	0.000	—	−0.004	−0.002	0.002
	761	0.000	0.000	0.000	—	−0.001	0.004	0.000
	921	0.004	0.003	0.003	—	0.003	−0.004	0.001
42	664	−0.001	−0.001	−0.001	—	0.005	0.003	−0.001
43	754	0.000	0.000	−0.002	—	−0.001	−0.004	−0.004
	930	−0.005	−0.004	−0.002	—	0.001	0.004	−0.004
	851	0.001	−0.001	−0.002	—	−0.005	0.003	0.003
44	763	−0.001	0.000	0.000	—	−0.002	0.001	0.000
	932	0.002	0.001	0.001	—	−0.001	−0.001	0.000
45	844	0.001	0.001	0.002	—	0.005	0.004	0.003
46	770	0.002	0.002	0.005	—	0.003	−0.007	−0.005
	853	0.000	0.000	0.000	—	−0.003	0.002	0.002
	941	−0.001	0.000	−0.003	—	0.000	0.003	0.006
47	860	0.001	0.001	0.004	—	0.001	−0.006	−0.001
	1000	0.000	0.000	0.000	—	0.000	0.000	0.000
48	772	−0.002	−0.001	0.001	—	−0.001	−0.003	−0.001
	1011	0.003	0.002	−0.004	—	−0.005	−0.005	−0.006
49	862	0.001	0.001	0.001	—	0.004	−0.002	0.000
	1020	−0.002	−0.001	−0.001	—	0.000	0.001	0.000
50	943	−0.002	−0.001	0.000	—	−0.001	0.000	0.000
	950	0.000	0.000	0.000		0.000	0.000	0.000

the absolute values of α_{lmn} for the 42.0 at.% Pd alloy are small compared with those for the 28.5 at.% Pd alloy. The nature of the SRO parameters in the non-splitting cases are similar to each other and are only a little different from the parameters in the splitting cases. To investigate how the split diffuse maxima are reflected in α_{lmn}, the diffuse intensity map was synthesized using a limited number of these parameters. We have noticed that the sign and magnitude of higher-order parameters play an important role in the appearance of split diffuse maxima, although their absolute values are very small compared with those of the lower-order parameters.

A possible local atomic arrangement could be constructed using the observed SRO parameters and a simulation program (Suzuki *et al* 1982, Ohshima *et al* 1987). SRO parameters beyond the thirtieth shell were adjusted so as to fit the experimentally determined α_{lmn}-values for the atomic arrangements of $10 \times 10 \times 10$ FCC unit cells. For reference, one set of results for Cu–13.0 at.% Pd alloy is shown in figure 3: figure 3(*a*) for the ideally random arrangement in which all the α-values are fitted to

Table 3. The numbers N_1 of Pd–Pd atom pairs as first-nearest neighbours, the numbers N_2 of Pd–Pd atom pairs as second-nearest neighbours and the ratios N_2/N_1.

	8.0 at.% Pd		9.5 at.% Pd		13.0 at.% Pd		21.8 at.% Pd		28.5 at.% Pd		42.0 at.% Pd	
	Random	SRO	Random	SRO	Random	SRO	Random	SRO	Random	SRO	Random	SRO
N_1	169	155	245	178	440	220	1220	840	2006	1236	4402	3569
N_2	73	112	110	162	200	328	593	917	1011	1410	2207	2563
N_2/N_1	0.43	0.72	0.45	0.91	0.46	1.49	0.49	1.09	0.50	1.14	0.50	0.72

zero except for $\alpha_{000} = 1$, and figure 3(*b*) for the observed SRO structure. Pd atoms are represented by circles, and these are linked together by red and green solid lines to their first- and second-nearest neighbours, respectively. The computer-simulated α_{lmn} were compared with those determined by experiment, and one set of these parameters is shown in table 2 in order to see the agreement between them. This confirms that the agreement is fairly good. Similar results were found for other Cu–Pd alloys in this study.

The structural difference between the SRO and random states can be seen if a careful comparison of figures 3(*a*) and 3(*b*) is made and can be characterized by comparing the number of Pd–Pd atom pairs as the first-nearest neighbours (N_1) and those as the second-nearest neighbours (N_2). In table 3 we list all these values for the states in all the six samples. It is very clear that N_1 is higher in the random case than in the SRO case, but N_2 is higher in the SRO case than in the random case. In the random case, the ratio of N_2/N_1 for lower Pd contents deviates from the ideal value (0.50) owing to computing error. It is seen that in the SRO case the ratio is less than unity in the Cu–8.0 at.% Pd and Cu–9.5 at.% Pd alloys and is higher than unity in the Cu–13.0 at.% Pd, Cu–21.8 at.% Pd and Cu–28.5 at.% Pd alloys. However, in the Cu–42.0 at.% Pd alloy, the ratio is again less than unity. On the basis of Hashimoto's (1974) model, it can be deduced that tiny Cu_3Au-type ordered regions exist in the disordered matrix and are correlated with each other if the split diffuse maxima appear in the diffraction pattern. Although we have tried to find such structural characteristics in the simulated models for the splitting cases, it was hard to define the boundary of the ordered regions in the disordered matrix.

Our main aim was to study the shape of diffuse scattering from Cu–Pd alloys with less than 13.0 at.% Pd and the nature of diffuse scattering from Cu–42.0 at.% Pd alloy. In Cu–Pd alloys with less than 13.0 at.% Pd, diffuse intensities were observed with no splitting. We previously thought that the separation of the split diffuse maxima would be very small and may be due to a weak diffuse intensity and less angular resolution. This is the first time that the SRO diffuse intensity from Cu–42.0 at.% Pd alloy has been measured quantitatively and no different feature in the SRO structure was observed for this alloy in comparison with the other alloys. We are, therefore, considering measuring the temperature-dependent diffuse intensities from Cu–42.0 at.% Pd alloy in order to understand the phase transition. Finally we expect our experimentally determined SRO parameters to be taken into account when calculating the band-structure energy in disordered Cu–Pd alloys.

References

Gyorffy B L and Stocks G M 1983 *Phys. Rev. Lett.* **50** 374

Hashimoto S 1974 *Acta Crystallogr.* A **30** 792

Koga K and Ohshima K 1990 *J. Phys.: Condens. Matter* **2** 5647

Krivoglaz M A 1969 *Theory of X-ray and Thermal Neutron Scattering by Real Crystals* (New York: Plenum)

Massalski T B, Okamoto H and Subramanion P K 1990 *Binary Alloy Phase Diagrams* vol 2 (Materials Park: ASM International) p 1454

Ohshima K, Iwao N and Harada J 1987 *J. Phys. F: Met. Phys.* **17** 1769

Ohshima K and Watanabe D 1973 *Acta Crystallogr.* A **29** 520

Ohshima K, Watanabe D and Harada J 1976 *Acta Crystallogr.* A **32** 883

Pearson W B 1958 *A Handbook of Lattice Spacings and Structures of Metals and Alloys* (Oxford: Pergamon)

Rao R S, Bansil A, Asonen H and Pessa M 1984 *Phys. Rev.* B **29** 1713

Suzuki H, Harada J, Matsui M and Adachi K 1982 *Acta Crystallogr.* A **38** 522

Takano N, Imai S and Fukuchi M 1991 *J. Phys. Soc. Japan* **60** 4218